AIAA JOURNAL
Vol. 43, No. 7, July 2005

Control of Vortical Flow over a Rounded Leading-Edge Delta Wing

Florent Renac,* Didier Barberis,† and Pascal Molton*
ONERA, 92190 Meudon, France

An attempt is made for fluidic control of the vortical flow and its related vortex breakdown phenomenon over a delta wing with a particular geometry. The model has a sweep angle of $\Lambda = 60$ deg and a rounded leading edge. The control system is based on four rectangular slots along the portside leading edge, and it provides continuous or pulsed jets normal to the leading-edge surface and parallel to the leeward side plane. The mass flow rate and the frequency of injection can be varied independently. The results are compared to a reference case defined by a microflap fixed along the leading edge and set perpendicular to it. Qualitative measurements are obtained with surface flow visualizations and boundary-layer transition detections with acenaphten. Quantitative data consist in mean and instantaneous surface pressure distributions measurements under the primary vortex axis and in mean three-dimensional velocity held measurements. The control effect is analyzed by means of laser sheet visualizations to detect the vortex breakdown position and by normal force and rolling moment measurements with a five-component balance.

Nomenclature

C_l	=	rolling moment coefficient
C_N	=	normal force coefficient
C_p	=	pressure coefficient
C_μ	=	blowing coefficient, $\dot{m}_j V_j / q_0 S_w$
c	=	root chord length
e	=	local semispan
f	=	blowing frequency
$\dot{m}_j$	=	mass flow rate of the control jet
p	=	static pressure
p_b	=	stagnation pressure of the control jet
p_0	=	freestream static pressure
q_0	=	dynamic pressure, $\rho_0 U_0^2/2$
Re_c	=	Reynolds number with respect to root chord length and freestream velocity
S_w	=	delta wing surface, $c^2 \tan\Lambda$
U, V, W	=	mean velocity components in the X, Y, and Z directions
U_0	=	freestream velocity
V_j	=	mean exit velocity of the control jet
X	=	chordwise distance from wing apex
X_b	=	vortex breakdown location from wing apex
Y	=	wing span distance from root chord
Y_c	=	spanwise position of the primary vortex axis
Z	=	distance from upper side
α	=	angle of attack, incidence angle
Λ	=	sweep angle
Ω_x	=	axial vorticity

Introduction

TODAY'S military aircraft and missile systems are expected to perform at high speed and high angle of attack. Demands for systems that are more maneuverable and more stealthy have encouraged the development of new concepts for the control of the separated flowfield and its associated vortical structure at extreme flight conditions. Many of the recent active control techniques involve the fluidic manipulation of the flowfield at the nose or around the fuselage. They consist in blowing, suction, or alternate actions at the leading edge or on the leeward side of the model. The basic idea of these control techniques is that a small and localized pneumatic control (suction and/or blowing) can modify the global parameters of the flow (lift, drag, noise, signature, stability, etc.) with a little additional energy consumption.[1–5] Moreover, these systems can be used to replace the traditional flaps and, thus, to obtain a significant reduction of the radar cross section.

Wood and Roberts[6] examined the control of the vortex breakdown by means of a continuous tangential mass injection at the rounded leading edge of a $\Lambda = 60$ deg sweep delta wing and proved the possibility for increasing the lift and extending the regime of stable vortical flow by approximately 11-deg angle of attack with a low blowing coefficient of $C_\mu = 5 \times 10^{-2}$. In the same way, Gu et al.[7] proved that an alternate suction–blowing in the tangential direction along a rounded leading edge can shift the vortex breakdown location downstream and delay the stall of the wing with a value $C_\mu = 9.7 \times 10^{-3}$. Barberis et al.[8] analyzed the applicability of the vortex breakdown control on a swept wing with a rounded leading edge by injecting pulsed or continuous jets in the feeding sheet. The results showed the efficiency of a pulsed jet normal to the boundary layer and highlighted the influence of the frequency of pulsation on the phenomenon. However, these systems are still costly for autonomic flight tests.

As an alternative to fluidic control, many studies proved that it is possible to create a rolling moment by placing a microflap at the rounded leading edge of the wing.[9–11] The magnitude and sign of the rolling moment could be varied through the location of the microflap around the leading edge, that is, its position according to that of the primary separation line. For a rounded leading edge, the separation line position evolves from the lower side toward the upper surface when increasing the angle of attack or decreasing the freestream Reynolds number. Jiang et al.,[12] thus, developed probes for measuring shear stress and determining the location of the separation line. Then, microflaps and baloons were used to set its position and create a rolling moment. A flight test was successfully experimented following the results obtained on the microelectromechanical systems vortex control.[13]

The first objective of this study is to provide new measurements on a delta wing with a particular geometry. Its low sweep angle and its rounded leading edge indeed make this model more representative of a real fighter aircraft than more slender wings with a sharp

Presented as Paper 2003-4008 at the AIAA 33rd Fluid Dynamics Conference, Orlando, FL, 23–26 June 2003; received 24 December 2003; revision received 12 October 2004; accepted for publication 29 December 2004. Copyright © 2005 by the authors. Published by the American Institute of Aeronautics and Astronautics, Inc., with permission. Copies of this paper may be made for personal or internal use, on condition that the copier pay the $10.00 per-copy fee to the Copyright Clearance Center, Inc., 222 Rosewood Drive, Danvers, MA 01923; include the code 0001-1452/05 $10.00 in correspondence with the CCC.

*Research Engineer, Fundamental and Experimental Aerodynamics Department, 8 rue des Vertugadins.

†Research Engineer, Fundamental and Experimental Aerodynamics Department, 8 rue des Vertugadins. Member AIAA.

leading edge. In the latter case, the primary separation line is fixed by the leading-edge singularity, and the vortical flow becomes two dimensional as Λ is increased. Practical wing design also incorporates a blunt leading edge,[14] where vortex flows are sensitive to Reynolds number. The second objective is to affect the global properties of the wing flowfield by applying a fluidic control. This flow is dominated by two steady counter-rotating vortices resulting from the separation of the boundary layer at the leading edge and from the rolling up of the formed shear layer. A part of the aerodynamic forces arises from this separated vortical flow over the wing. The control is applied in the leading-edge region to alter the separation process and, thus, to modify the vortical structure and the related aerodynamic properties of the wing. Moreover, it is located at the portside of the model to make the flow asymmetric and, thus, to create a rolling moment. From an application point of view, the mass flow rate required for the blowing is acquired from the jet engines, so one would generate the control of the flow with a minimum mass flow rate.

This paper is organized as follows: A brief description of the experimental conditions and techniques is given in the next section. The subsequent section presents a characterization of the vortical flowfield over a rounded leading-edge delta wing in nominal configuration, that is, without blowing. In the following section, the vortical flowfield is perturbed by means of the control system with a reduced blowing coefficient $C_\mu < 5 \times 10^{-3}$ for the pulsed blowing and $C_\mu < 2 \times 10^{-2}$ for the steady blowing. As a reference case, control with a microflap located on the leading edge is also explored. Finally, new results are summarized in the last section.

Experimental System and Technique

All experiments reported in this paper were conducted in the F2 subsonic, closed-return, and atmospheric wind tunnel at ONERA's Fauga-Mauzac Center. The test section is rectangular with a width of 1.4 m, a height of 1.8 m, and a length of 5 m (Fig. 1). The turbulence levels are estimated to be less than 0.1% of the freestream velocity U_0, and the flow is uniform across the test section to within 1% (Ref. 15). The delta wing model is mounted on a sting with a horizontal support and a stub axle for adjusting the angle of attack. The horizontal support is manipulated in height along a vertical column to maintain the wing close to the center axis of the test section.

The delta wing model possesses a rounded leading edge, a sweep angle of $\Lambda = 60$ deg, and a root chord length of $c = 690$ mm. The model has a wingspan of 804.7 mm at its trailing edge, is 40 mm thick, and is beveled on the windward side at an angle of 15 deg to form a rounded leading edge with a radius of curvature equal to 6.9 mm. A schematic of the model is given in Fig. 2. The sting that supports the model is mounted 540 mm behind the apex in the symmetry plane of the wing and on the lower surface (Fig. 1).

The experimental control device is based on four rectangular slots that are 50 mm long, 0.25 mm wide, and evenly spaced out 20-mm apart along the leading edge. They are labeled slots 1–4 with increasing distance from the apex (Fig. 2), and the nondimensional abscissas of their centers are $X_i/c = 0.33, 0.41, 0.50$ and 0.59, respectively. They provide continuous or pulsed jets normal to the

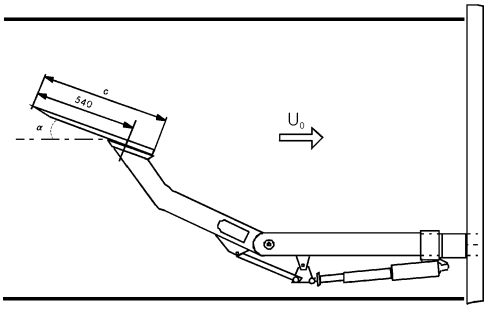

Fig. 1 Lateral view of test section (dimension in millimeters).

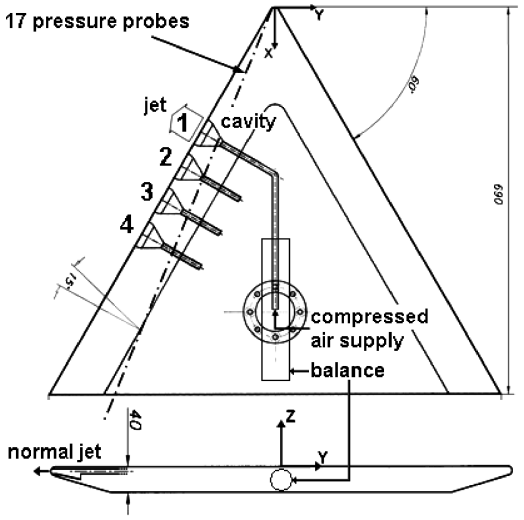

Fig. 2 Top and rear views of delta wing model (dimensions in millimeters) and Cartesian frame *X*, *Y*, and *Z*.

leading-edge surface and parallel to the leeward side plane. A rotating system, driven by an ac motor, enables the supply of pulsed air to the slots. The blowing frequency f and the mean mass flow rate $\dot{m}_j$ are modifiable through the rotation rate of the motor and through the pressure supply, respectively. The mean blowing coefficient $C_\mu = \dot{m}_j V_j / q_0 S_w$ is used to compare the mean momentum flux of the control jet to a measure of the freestream momentum flux. The mass flow rate is estimated by means of a conical throat and by assuming isentropic laws[16] as well as conditions of sonic jet at the slot exit.

The results are obtained for various angles of attack ranging between $\alpha = 5$ and 35 deg and for four freestream velocities, $U_0 = 25$, 34, 50, and 75 m/s. The corresponding freestream Reynolds numbers based on the root chord length and on the freestream velocity are $Re_c = U_0 c/\nu = 1.2 \times 10^6$, 1.6×10^6, 2.3×10^6 and 3.5×10^6, respectively. The boundary-layer transition is not controlled during these experiments.

Laser Sheet Visualizations

The laser sheet visualization are accomplished with a 15-W argon laser. Theater smoke (P/Smog FS25) is generated in a commercial smoke machine, then entrained into the freestream flow downstream of the model, and subsequently filled the closed-return circuit. During the tests, the laser sheet is directed to intersect the separated flow regions, and the results are captured by either a 35-mm camera or a video camera positioned perpendicular to the laser sheet. The streamwise distance X_b of the breakdown location from the apex of the wing is measured directly from the recorded laser sheet images by means of an automatic location method.[17] These values are then divided by the root chord length, measured from the same images, thus providing nondimensional length X_b/c. A global measurement uncertainty for the values of X_b/c is estimated to be of the order of 2.5% over the wide range of angles of attack.

Surface Flow Visualizations

Oil flow visualizations were accomplished with a viscous coating composed of paraffin oil, zinc titanium, and oleic acid. The model surfaces were covered with a thin layer of this mixture. Skin friction caused the viscous coating to build up in certain areas and to stretch in others. The evolution of the oil flow is recorded on video, and photographs are taken at the end of each test run with and without the application of the flow control technique. When the topology of the oil streaks is interpreted with the use of the critical point theory and some details of the flowfield above the surface are interpreted, a correlation between the vortical flowfield and the surface skin-friction pattern can be established.[18]

Acenaphten is a mixture of acetone and naphthalene and consists of a white powder, which is put on the model surface. This product sublimates when exposed to intense friction as in the turbulent regime. The product disappears, and thus, dark areas represent zones of turbulent flow regime. The acquisition method is the same as for the oil flow visualizations. Particular precautions must be taken because this product is sensitive to external conditions such as freestream temperature.[19]

Laser Doppler Velocimetry

Laser Doppler velocimetry (LDV) is a nonintrusive technique for measuring the local velocity in a flowfield. The three-dimensional LDV system at ONERA utilizes two 15-W argon lasers as sources of light and operates in the forward scattering mode. For each volume of exploration, the three instantaneous velocity components related to a specific particle are acquired. The average and the standard deviation of the velocity component in each of the three directions are then calculated from a sample of 2000 particles. The global accuracy of the mean velocity components is estimated to be less than 1.5% by assuming an absolute error of the angle between the velocity vector and a plane of reference. The measurements were repeatable, and angles were always smaller than the estimated error assumption, thus leading to an estimated accuracy of the magnitude of the velocity to ± 1 m/s and of the direction of the velocity vector to ± 1 deg (Ref. 20).

Mean and Instantaneous Surface Pressure Measurements

There are 17 differential pressure transducers (Kulite, Type XCQ-093-2D) located on the leeward side of the model and under the position of the axis of the portside primary vortex. This position is determined from laser sheet visualization at $\alpha = 18$ deg and $Re_c = 2.3 \times 10^6$. They are evenly spaced between the chordwise distances $0.14 < X/c < 0.98$. Because pressure measurements are conducted for a range of incidences $5 < \alpha < 33$ deg, the vortex axis is shifted in the spanwise direction between the nondimensional positions $0.58 < Y_c/e < 0.77$. It has a position $Y_c/e = 0.71$ for $\alpha = 18$ deg.

Forces and Moment Measurements

A five-component balance is used to measure the aerodynamic force normal to the wing surface as well as the rolling moment. The diameter of the balance is 30 mm and its length is 310 mm. Flexible tubes are used for the air supply of the blowing slots to minimize the induced effects of the control on the measurements.

Nominal Configuration Results

Surface Flow Visualizations

To better understand the vortical flowfield phenomenon, one can observe the traces of the skin-friction lines on the leeward surface of the delta wing. Results are shown in Figs. 3 and 4. Contrary to results obtained for sharp edged delta wings,[1,16] the primary separation line S_1 of the boundary layer coming from the lower surface is not rectilinear along the leading edge of the wing. As shown in Fig. 3, its position is close to the upper surface at the apex and moves toward the lower surface when going away from the apex. This agrees with results of Jiang et al.[12] on a $\Lambda = 56.5$ deg sweep delta wing with a rounded leading edge on which the position of the boundary-layer seperation was found to describe a curved line. Moreover, they found

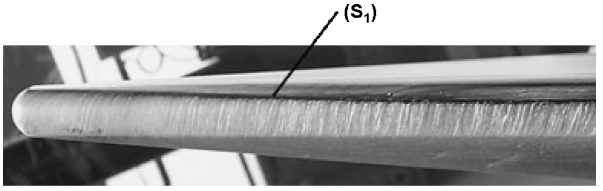

Fig. 3 Surface oil flow visualization at $\alpha = 20$ deg and $Re_c = 2.3 \times 10^6$ (nominal configuration); detail of left leading edge.

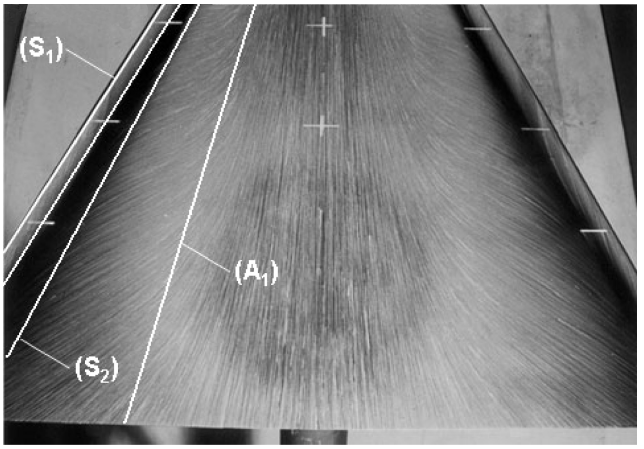

Fig. 4 Surface oil flow visualization at $\alpha = 20$ deg and $Re_c = 2.3 \times 10^6$ (nominal configuration); upper side view.

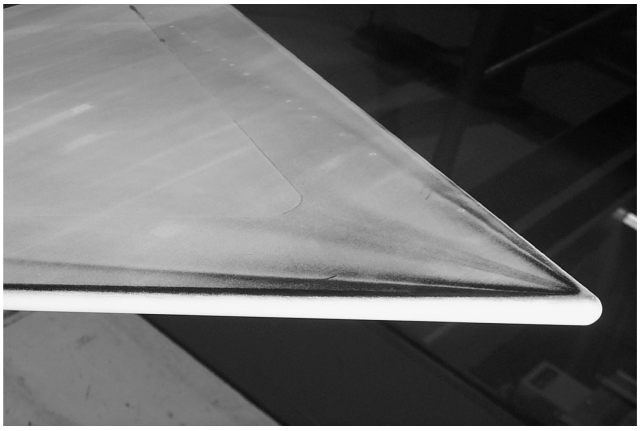

Fig. 5 Visualization of boundary layer transition with sublimating product at $\alpha = 20$ deg and $Re_c = 2.3 \times 10^6$ (nominal configuration).

that S_1 moves toward the lower surface with increasing freestream Reynolds number due to a higher pressure gradient.

The separated shear layer rolls up into a conical structure over the upper surface of the wing and meets it at the primary attachment line A_1. This line represents a boundary between two zones. The first zone stays between the two attachment lines A_1 and corresponds to skin-friction lines parallel to the root chord. In the second zone, the traces converge on the secondary separation line S_2. The average position of the primary vortex axis stays between A_1 and S_2 but very close to S_2. The shear layer separating at S_2 rolls up and produces a secondary vortex that reattachs at the secondary attachment line A_2. The effects of the secondary vortices on the upper surface appear between A_2 and S_2 with skin-friction lines directed from each leading edge toward the center line. This feature characterizes the counter rotation of the secondary vortex with respect to the primary vortex. The patterns do not denote any trace of the primary vortex breakdowns and, thus, confirm previous results,[4] which showed that surface oil flow visualizations do not constitute a reliable method for identifying the vortex breakdown location.

Figure 5 presents the transition lines of the boundary layer in a region close to the apex of the wing. The flow remains laminar on a large part of the wing characterized by white surfaces. Especially, the boundary layer is laminar on the rounded leading edge. The dark lines are associated with the primary and secondary separation lines (determined from analysis of the viscous flow visualizations) and extend from the apex to the trailing edge. The transition of the boundary layer occurs at the separation line, but it becomes laminar when it reattaches at the wing as illustrated by the white regions between A_1 and S_2 or between A_2 and S_1.

Laser Sheet Visualizations

A series of laser sheet visualizations were conducted at angle of attack ranging from 10 to 30 deg and for a freestream Reynolds number of $Re_c = 2.3 \times 10^6$. As an example, Fig. 6 presents such a visualization of the flowfield in the upstream region. Note that the average values of the portside and starboard breakdown locations are systematically measured. (The results are not shown here.) They provide a recurrent discrepancy: The right breakdown location is indeed always aft of the left one. This difference seems to be due to experimental uncertainties such as a small yaw angle of the wing in the test section with respect to the freestream velocity or a slight geometrical difference between both leading edges. The primary vortex core upstream of its breakdown appears as a dark region void of particles because of the centrifugal forces action, which is surrounded by a well-seeded and highly reflective flow. At the vortex breakdown location, there is a rapid expansion of the vortex core diameter. It leads to a reduction of the axial and azimuthal velocities as consequence of the mass and circulation conservation and, thus, to a stagnation flow region where the vortex particles are evenly dispersed throughout the laser sheet. For each freestream condition, instantaneous nondimensional vortex breakdown locations X_b/c are analyzed for 80 frames and averaged to determine each of the mean values.

Each vortex core follows a path that begins at the wing apex and continues along an average sweep angle of 66 deg until it reaches the trailing edge, where it turns in the direction of the freestream flow. The vortex breakdown positions are seen to be roughly independent of the Reynolds number, as seen in Fig. 6. The effect of the angle of attack is presented in Fig. 7. Results are given for the current tests ($Re_c = 2.3 \times 10^6$) and for previous experiments on two delta wings with a sharp leading edge and beveled at an angle of 15 deg on the windward side. One wing has a sweep angle of $\Lambda = 70$ deg (Refs. 1–4) and $Re_c = 1.5 \times 10^6$, and the other model is a $\Lambda = 60$ deg sweep delta wing[21] and results are acquired for $Re_c = 10^6$.

In the case of our model, the vortex breakdown occurs beyond the trailing edge for $\alpha < 12$ deg. This comparison holds because the vortex breakdown position is roughly independent of the Reynolds number for high values of Re_c. For greater incidences, one can observe the obvious upstream shift of the vortex breakdown location from the trailing edge toward the apex as α is increased. For $13 < \alpha < 25$ deg, the behavior of the breakdown location is close to a linear and rapid evolution, whereas for $\alpha > 25$ deg, the vortex breakdown remains in the neighborhood of the apex and its progression seems to be slowed. The comparison with other experiments confirms some general trends. In the one hand, the vortex breakdown position moves upstream over the wing as the sweep angle is decreased.[22] Moreover, one can see that the slope of the breakdown location evolution with α is the same for both results with sharp leading edges. An increase in sweep angle appears merely to shift the breakdown position downstream without changing its evolution. In the other hand, the leading-edge shape is seen to modify both the breakdown position and its evolution. Compared to a rounded leading edge, a sharp one accelerates the breakdown evolution toward the apex. For low angles of attack ($\alpha < 25$ deg), X_b/c is lower for the rounded leading edge, indicating an earlier breakdown over the leeward side, whereas this trend is inverse for great angles of attack ($\alpha > 25$ deg).

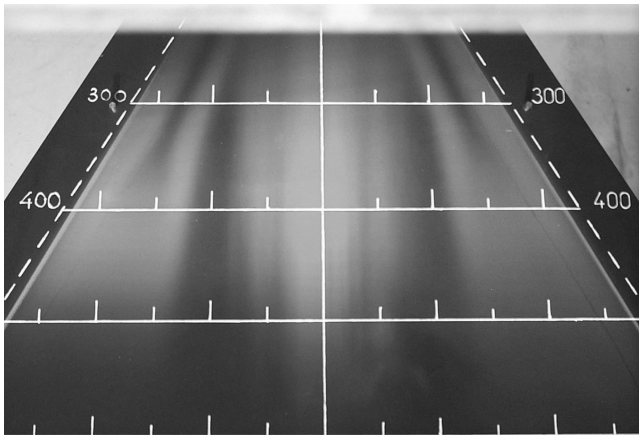

Fig. 6 Laser sheet visualization in longitudinal plane at $\alpha = 18$ deg and $Re_c = 2.3 \times 10^6$ (nominal configuration).

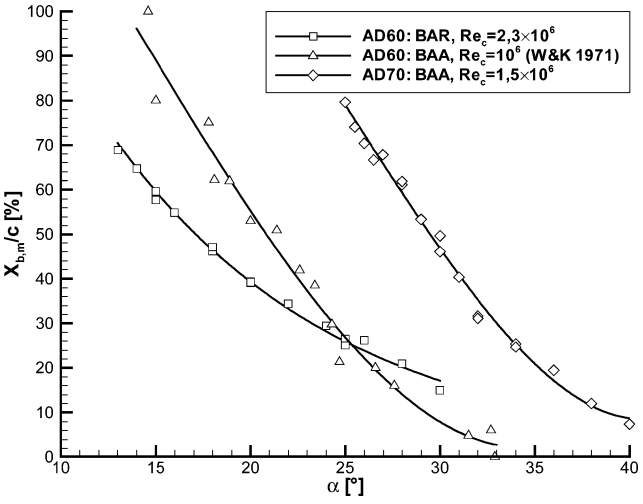

Fig. 7 Evolution of X_b/c as function of α for three delta wing models $\Lambda = 60$ deg, rounded leading edge, $Re_c = 2.3 \times 10^6$; $\Lambda = 60$ deg, sharp leading edge,[2] $Re_c = 10^6$; and $\Lambda = 70$ deg, sharp leading edge,[4] $Re_c = 1.5 \times 10^6$.

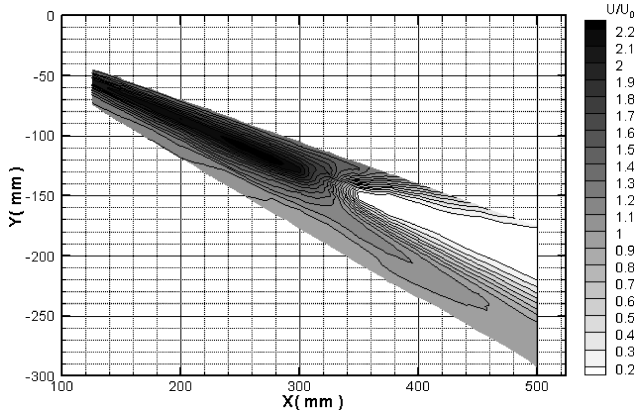

Fig. 8 Contours of nondimensional axial velocity U/U_0 in the longitudinal plane; $Re_c = 2.3 \times 10^6$ and $\alpha = 18$ deg.

LDV

The following results concern the portside flowfield over the wing. The domain explored is constituted by two transverse planes perpendicular to the root chord of the model that are located at $X = 250$ and 350 mm ($X/c = 0.36$ and 0.51) and by one longitudinal plane following the axis of the vortex core. Each perpendicular mesh contains approximately 1200 points evenly spaced out $\Delta Y = \Delta Z = 2$ mm apart. The longitudinal plane is located between the stations $X = 125$ and $X = 500$ mm ($0.18 < X/c < 0.72$) and is constituted by 535 points. The mesh points spacing is $\Delta X = 25$ mm in the longitudinal direction and $\Delta Y = 2$ mm in the spanwise direction. The data were acquired with freestream conditions of $\alpha = 18$ deg and $Re_c = 2.3 \times 10^6$, which corresponds to a mean breakdown location of $X_b/c = 0.47$ between both transverse measurement planes.

Figure 8 presents the contours of the nondimensional longitudinal velocity U/U_0 in the streamwise plane. Upstream of the vortex breakdown location, the flow has a jetlike profile characterized by a strong acceleration of the flow with values reaching $U/U_0 = 2.2$ in the vortex core. The balance between the radial pressure gradient and the centrifugal force induces a drop near the axis.[23] According to Hall,[22] this drop is reinforced downstream because of the

continuous feeding from the entire leading edge. The conical shape of the flowfield imposes an equilibrium between centrifugal and axial momentum, thus leading to an increasing axial velocity toward the axis as well as in the downstream direction. In the neighborhood of the breakdown location, the values of the axial velocity quickly decrease, indicating that the flow slows down and that the size of the vortex core increases. A stagnation zone with velocities close to zero follows this region. The axial velocity field develops from a jetlike velocity profile upstream of the breakdown location to a wake-type profile downstream of it. This feature is characteristic of vortical flows with presence of burst.[24,25] However, the recirculation zone is absent: The axial velocities stay always positive, even if they are small. Moreover, the evolution from a well-developed vortex to a disorganized one is not abrupt, contrary to the most of the experiments on delta wings.

Contours of the axial vorticity component $\Omega_x c/U_0$ in the two transverse planes are presented in Fig. 9. The axial vorticity Ω_x is calculated from the mean velocity components measured in each plane and from a central differential scheme to evaluate the derivatives. Each plane reveals three highly rotational zones in the flowfield. First, the leading-edge vortex core presents strong negative vorticity levels before breakdown. The shear layer issuing from the windward side and separating at the leading edge rolls up and accumulates vorticity in the vortex core. This is consistent with the great axial velocities on the axis upstream of breakdown (Fig. 8). From the breakdown position, the stream surfaces diverge and axial vorticity levels decrease to satisfy the conservation of angular momentum. Second, the shear layer separating from the leading edge also contains high levels of negative vorticity. The flow emanating from the lower side of the wing and the flow over the wing near the leading edge ineract. They consist of parallel streams and create a velocity gradient that produces rotation, thus supplying the mixing layer. Precedent experiments[26,27] have shown the existence of several isolated and steady vortical substructures in the feeding sheet for a wide variety of sweep angles, $55 < \Lambda < 85$ deg (Ref. 28). These have been attributed to a three-dimensional Kelvin–Helmoltz instability. Nevertheless, the current results do not contain these pockets of vorticity, as seen in Fig. 9. This feature is not clear, and one certainly must take into account the shape of the rounded leading edge, which allows a smoothly evolution of the shear layer compared to a sharp one and, thus, reduces the amplification of such instability. Finally, the contours of axial vorticity underscore the presence of the secondary vortex located between the shear layer, the primary vortex, and the leeward surface of the wing. The axial vorticity levels are likewise high in this zone and are positive, illustrating the counter rotation of the vortex compared to the primary vortex. Note that the secondary vortex, as well as the shear layer, remains qualitatively similar in both measurement planes. These regions seem not to be influenced by the vortex breakdown phenomenon.

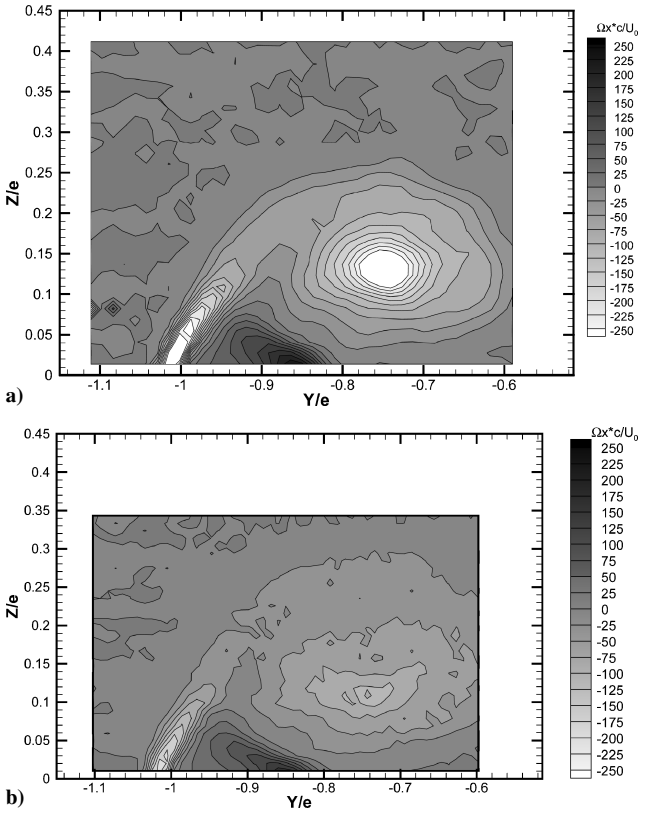

Fig. 9 Contours of the nondimensional axial vorticity $\Omega_x c/U_0$ for freestream conditions of $Re_c = 2.3 \times 10^6$ and $\alpha = 18$ deg (nominal configuration); coordinates are divided by the local semispan: transverse planes a) $X/c = 0.36$ and b) $X/c = 0.51$.

Mean and Instantaneous Surface Pressure Measurements

Figure 10 shows the evolution of the distribution of the mean pressure coefficient $C_p = (p - p_0)/q_0$ under the primary vortex axis as a function of the angle of attack. As a result, one can seen that an increase of α induces a depression toward the apex until $\alpha = 29$ deg. This trend corresponds to the intensification of the primary vortex with increasing α. At $\alpha = 33$ deg, the pressure levels strongly decrease. This phenomenon corresponds to stall and is characterized by a collapse of the lift force. Laser sheet visualization results (Fig. 7) show that the vortex breakdown occurs near the apex at this angle of attack and that the flowfield may be slowed on a large part of the wing. Note that, for lower values of the angle of attack, the vortex breakdown does not affect the evolution of the mean pressure coefficient and agrees with other experiments.[4] As an example, at $\alpha = 18$ deg the vortex breakdown occurs at $X_b/c = 0.47$ and the coefficient C_p increases regularly in the neighborhood of this station.

The power spectrums of the pressure fluctuations at a fixed incidence $\alpha = 18$ deg are represented in Fig. 11. Sensor 7 ($X_7/c = 0.47$) is located just under the vortex breakdown point, whereas the three other sensors are located downstream of it. The two downstream sensors 13 ($X_{13}/c = 0.69$) and 15 ($X_{15}/c = 0.80$) exhibit a bump that does not appear for the upstream sensors. Moreover, this bump is not centered on the same frequency for each sensor. This phenomenon has been already observed in earlier experiments[29,30] and is related to the helical mode instability.[31] A recent linear temporal and inviscid instability analysis applied on LDV measurements on primary vortices over delta wings with different geometries shows the existence of ring modes (Ref. 32) in the breakdown wake constituted by an infinite family of negative helical modes. These ring modes exhibit high frequencies compared to the intrinsic vortex frequency scale and develop around a critical radius that increases with the abscissa X/c. The bump in the power spectra could, therefore, be the signature of this instability when its critical radius is sufficiently great to reach the leeward side. Nevertheless, there is no velocity measurement plane at this abscissa to check this assumption.

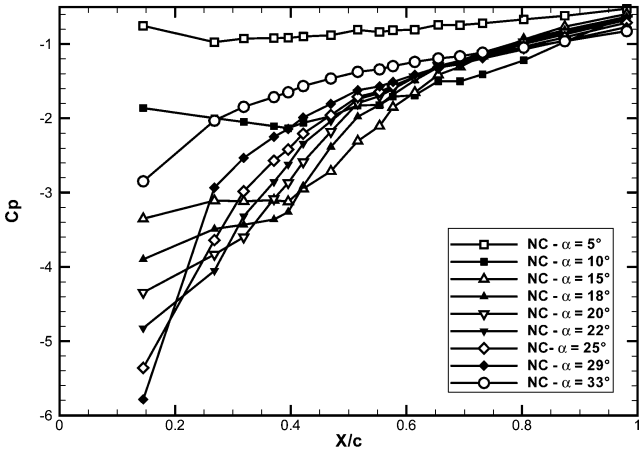

Fig. 10 Longitudinal distributions of the mean pressure coefficient C_p as function of α for $Re_c = 2.3 \times 10^6$ (nominal configuration).

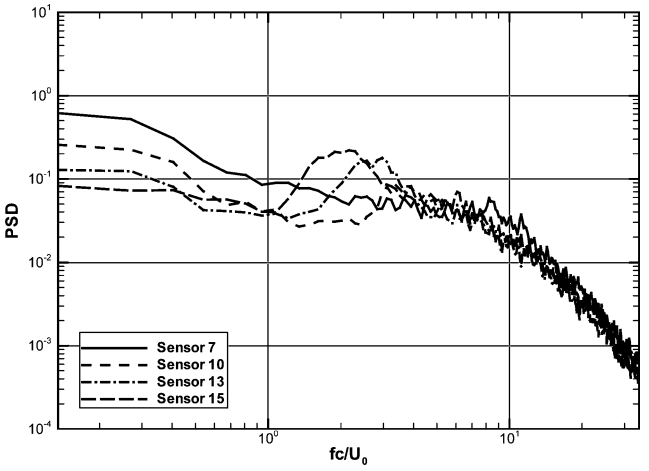

Fig. 11 Frequency power spectra of pressure fluctuations at four locations; $X_7/c = 0.47$, $X_{10}/c = 0.58$, $X_{13}/c = 0.69$, and $X_{15}/c = 0.80$ for $Re_c = 2.3 \times 10^6$ and $\alpha = 18$ deg (nominal configuration).

Force and Moment Measurements

The evolutions of the aerodynamic coefficients of normal force C_N and rolling moment C_l are shown in Fig. 12 as a function of the angle of attack and for four distinct freestream Reynolds numbers. The force and moments are made nondimensional by using the freestream dynamic pressure q_0, the wing surface S_w and the root chord length c. For low angle of attack $\alpha < 10$ deg, the C_N increases linearly with α as predicted by the potential theory. For greater incidences, the vortex strength becomes significant and contributes to an increase of the aerodynamic force as seen by the increase in the slope of the curve (C_N, α). The maximum of C_N is reached for $\alpha = 30$ deg. At this incidence, the vortex breakdown reaches the wing apex and the characteristics of the flowfield change dramatically. The evolution of the rolling moment coefficient is more complicated. Finally, the aerodynamic coefficients are independent of the Reynolds number variation. For each configuration, C_l keeps low values over the most part of the angle-of-attack range.However, at some incidences, $\alpha = 10$ and $\alpha = 26$ deg, the rolling moment changes signs. The reasons of this behavior are not clear because C_l is zero for a strictly symmetric flow. One can observe that at $\alpha = 10$ deg vortex breakdown occurs near the trailing edge of the wing and that at $\alpha = 26$ deg vortex breakdown reaches apex (Fig. 7).

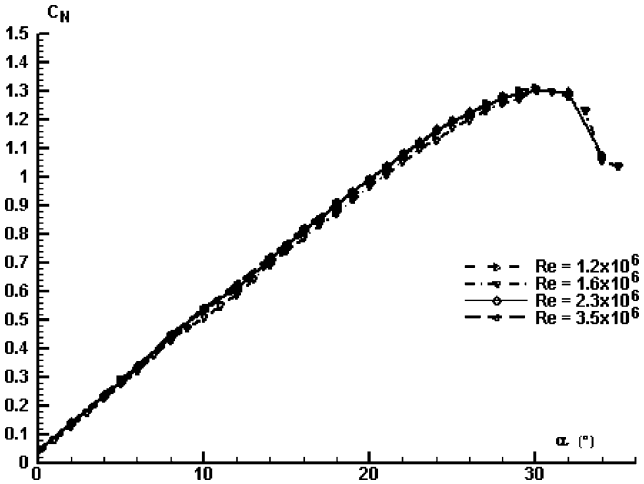

a) Normal force coefficient

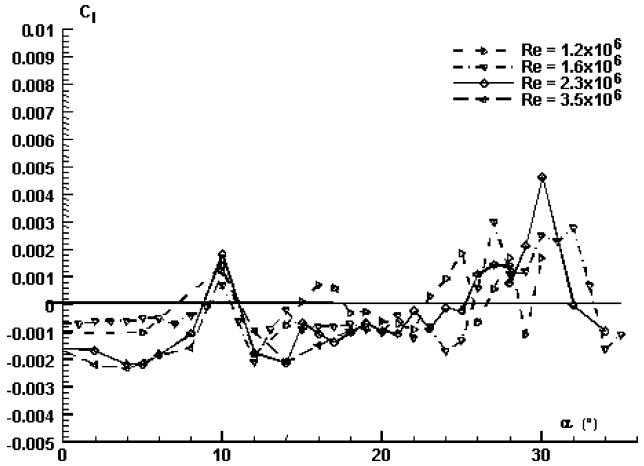

b) Rolling moment coefficient

Fig. 12 Aerodynamic normal force and rolling moment coefficients evolutions as a function of α for various Reynolds numbers $Re_c = 1.2 \times 10^6$, 1.6×10^6, 2.3×10^6, and 3.5×10^6 (nominal configuration).

Control Configuration Results

Here we explore the flow subjected to different controls. We first present the flap control results as a reference. We then analyze the effects of pulsed and continuous blowings.

Microflap Control

Force and Moment Measurements

Figure 13 shows the effect of the microflap on the rolling moment coefficient C_l as a function of the angle of attack for three configurations depending on the length of the microflap along the leading edge. (See the Fig. 13 caption.) Part A of the flap covers the upstream part of the leading edge ($X/c < 0.30$); part B covers the median region, which corresponds to the four slots position ($0.30 < X/c < 0.63$); and part C covers the downstream part ($X/c > 0.63$). The microflap is placed perpendicular to the leading edge and parallel to the leeward side, and its width is 2 mm. The maximum rolling moment is achieved with a flap along the entire leading edge (parts A, B and C, denoted full-length flap in the following paragraphs) for a large range of incidence angles $12 < \alpha < 30$ deg. When only part B of the flap is used, the highest value of the rolling moment variation is obtained at $\alpha = 15$ deg, but it reduces with increasing incidence, that is, when the vortex breakdown location occurs upstream of part B. Thus, it appears that the flap has an influence on the rolling moment when it can interact with the vortex

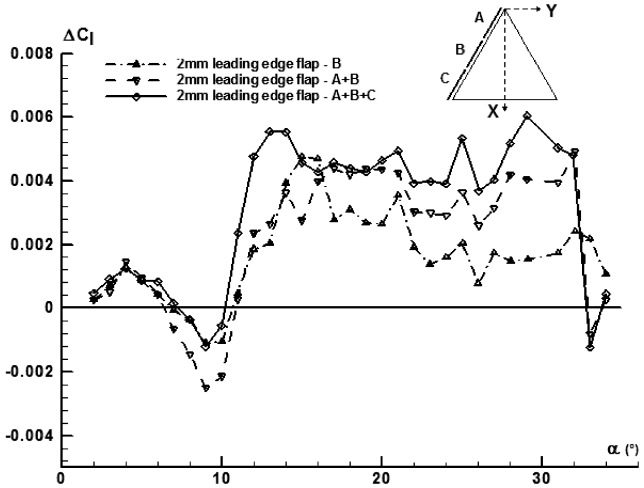

Fig. 13 Variation in rolling moment coefficient $\Delta C_l = C_l - C_{l,NC}$ compared to the nominal result $C_{l,NC}$ when a microflap is placed at the leading edge for $Re_c = 2.3 \times 10^6$; schematic of flaps A, B, and C along leading edge.

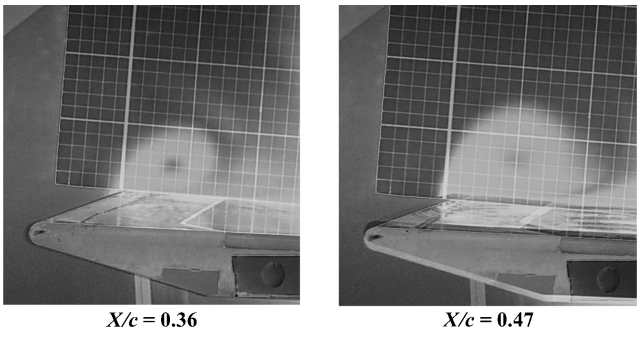

Fig. 14 $Re_c = 2.3 \times 10^6$, $\alpha = 18$ deg, laser sheet visualizations in four transverse planes a) without and b) with a full-length microflap at the leading edge.

breakdown. The interest of a full-length flap is, thus, to be adapted to all vortex breakdown positions, that is, whatever α. We, thus, will use this last configuration as a reference case for comparison with fluidic control.

Matsuno et al.[9] have studied the characteristics of the rolling moment on a $\Lambda = 45$ deg delta wing with a leading-edge flap. The wing has a root chord of $c = 160$ mm and a rounded leading edge with a radius of curvature of 7.25 mm. The flap is placed along the leading edge between the abscissas $0.10 < X/c < 0.75$, with a width of 2 mm. It can produce a rolling moment coefficient variation of $\Delta C_l = \pm 10^{-2}$, which is sufficient for flight control. In our case, the maximum rolling moment variation is obtained for two incidences $\alpha = 13$ and 29 deg, with a value of $\Delta C_l = 6 \times 10^{-3}$, and we retain it as a reference. According to the authors,[9] the delta wing used for their study produces relatively weak primary vortices that are easily broken by small disturbances. Thus, the microflap could be less effective on more slender wings where primary vortices are stronger.

Laser Sheet Visualizations

Figure 14 presents laser sheet visualizations at two stations, $X/c = 0.36$ and 0.47. The former is located upstream of the vortex breakdown position, whereas the latter is downstream of it, in the nominal configuration as well as in the control configuration with the full-length flap. At $X/c = 0.36$, a second vortex develops near the leading edge in the presence of control. Furthermore, the primary vortex axis seems not to be shifted inboard contrary to other experiments of Huang et al.[13] In the downstream plane, $X/c = 0.47$, the second vortex cannot be observed, and the visualization with control is similar to that of the nominal configuration.

Pulsed Blowing Control: Surface Pressure Measurements

Figure 15 presents a comparison between the evolutions of the mean pressure coefficient C_p in the nominal configuration and in configurations with control pulsed blowing through the slot 1 for several values of the pulsed frequency f and for a fixed angle of attack $\alpha = 18$ deg. Compared to the nominal configuration, one can observe that each control configuration gives a lower value of C_p

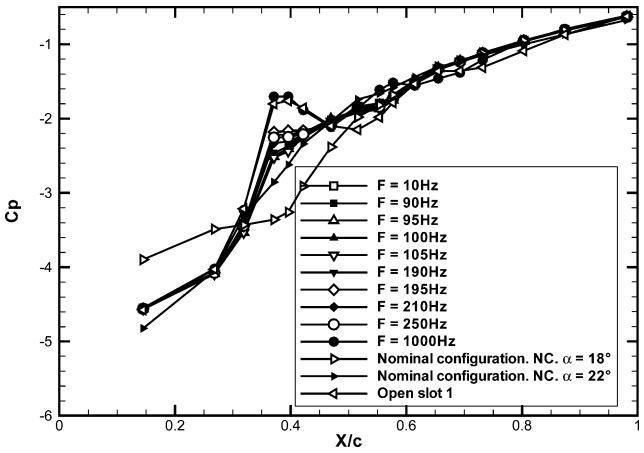

Fig. 15 Longitudinal distribution of mean pressure coefficient C_p as function of control frequency f for $Re_c = 2.3 \times 10^6$ and $\alpha = 18$ deg; data compared to results obtained in nominal configuration for $\alpha = 18$ and 22 deg.

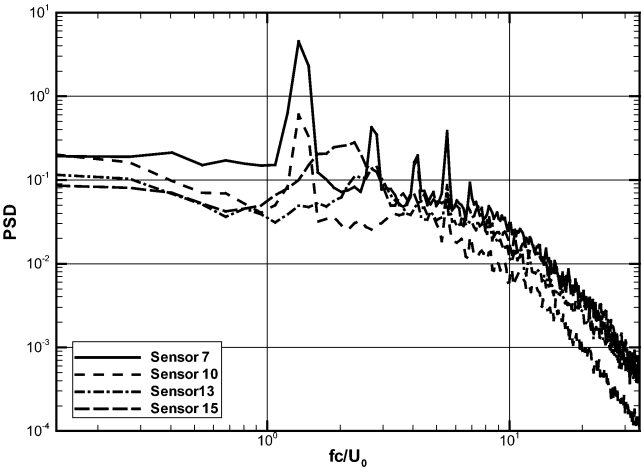

Fig. 16 Frequency power spectra of pressure fluctuations at four locations $X_7/c = 0.47$, $X_{10}/c = 0.58$, $X_{13}/c = 0.69$ and $X_{15}/c = 0.80$ for $Re_c = 2.3 \times 10^6$ and $\alpha = 18$ deg (normal pulsed blowing at $f = 100$ Hz through slot 2).

upstream of the control slot and a greater value in its neighborhood. Farther downstream, all results match. Except for measurements with $f = 1000$ Hz, there is no influence of the frequency. Note that the mass flow rate of the control jets decreases with the frequency and for the greatest frequency, $f = 1000$ Hz, it is close to zero.[33] For this frequency, we obtain the same results as for the configuration with slot 1 open without blowing. Finally, observe that the evolution of C_p for frequencies $10 < f < 250$ Hz obtained at $\alpha = 18$ deg are similar to the nominal results obtained at $\alpha = 22$ deg.

Figure 16 presents the evolution of the power spectral density (PSD) for a pulsed blowing at a frequency $f = 100$ Hz through slot 2. We consider four sensors located downstream of slot 2. The PSD distributions of the sensors 7 and 10 exhibit the fundamental excitation frequency, as well as the first harmonics. The amplitude of these peaks decrease when going away from the blowing slot, and the influence of the control disappears at sensors 13 and 15. Likewise, the bump observed in the nominal configuration (Fig. 11, sensors 10 and 13) is still present and is not modified by the presence of the control.

Steady Blowing Control

Surface Oil Flow Visualization

Figure 17 presents a leeward side view of the surface flow patterns subjected to a simultaneous continuous blowing through the four slots. The effect of the control could be analyzed by comparing

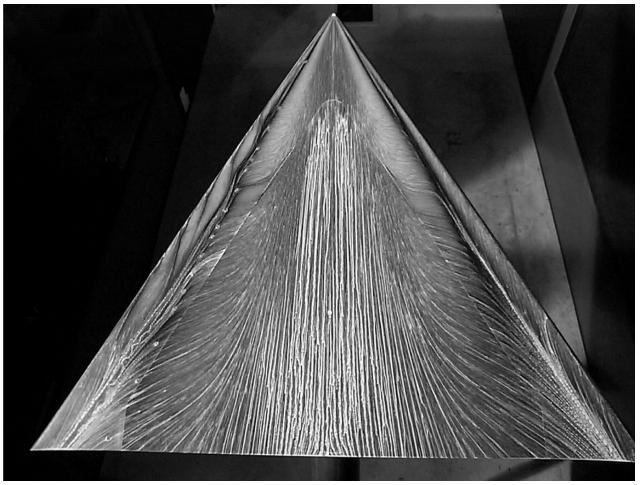

Fig. 17 Surface oil flow visualization in presence of continuous and normal blowing through four slots, $Re_c = 2.3 \times 10^6$ and $\alpha = 16$ deg.

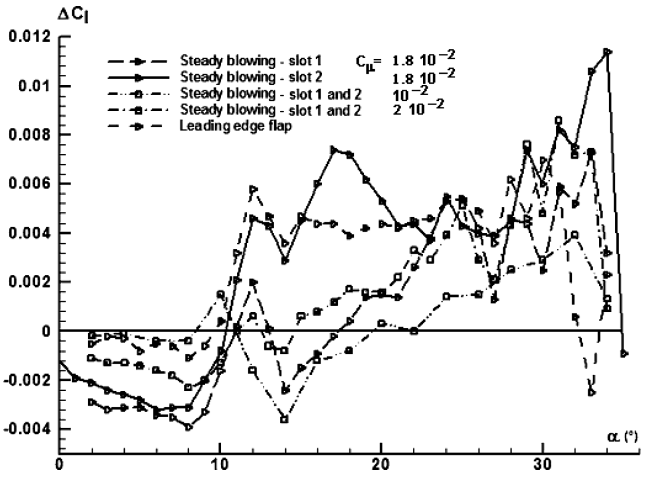

Fig. 18 Effect of a steady blowing on rolling moment coefficient; comparison with results obtained for full length flap, $Re_c = 1.6 \times 10^6$.

the left-hand side of the wing (with control) and its right-hand side (without control). As a result, some new local separation zones are formed near each slot. They result from the interaction between the control jet and the transverse freestream flow. They are delimited by two lines beginning at the start and at the end of each slot.

Forces and Moment Measurements

The rolling moment variations for different steady normal blowings are shown in Fig. 18 as a function of the angle of attack. Here, both the mass flow rate and the activated slot are varied, and we compare the results to those obtained with the full length flap. For a blowing pressure of $p_b = 4$ bar through slots 1 and 2 ($C_\mu = 10^{-2}$), no significant rolling moment can be achieved. By blowing through the same slots with a greater blowing pressure $p_b = 6.5$ bar ($C_\mu = 1.8 \times 10^{-2}$), one can observe a negative variation of the rolling moment for $\alpha < 10$ deg. For $\alpha > 15$ deg, the rolling moment changes sign and increases with α. Hong et al.[34] explains this change in the sign of ΔC_l by the formation and development of the primary vortices over the wing. For low incidences, the primary vortices are not formed and the rolling up of the blowing jet strengthens the portside vortical flow and, thus, creates a negative rolling moment. For higher incidences, the mechanism is not yet well understood. Blowing through slot 2 generates larger rolling moment with values comparable to that obtained with a full length flap. Greater changes in ΔC_l are even observable compared to this latter configuration for ranges of angle of attack $15 < \alpha < 21$ deg and $32 < \alpha < 35$ deg. Figure 19 presents the variation of the normal force coefficient as a function of α for the preceding configurations.

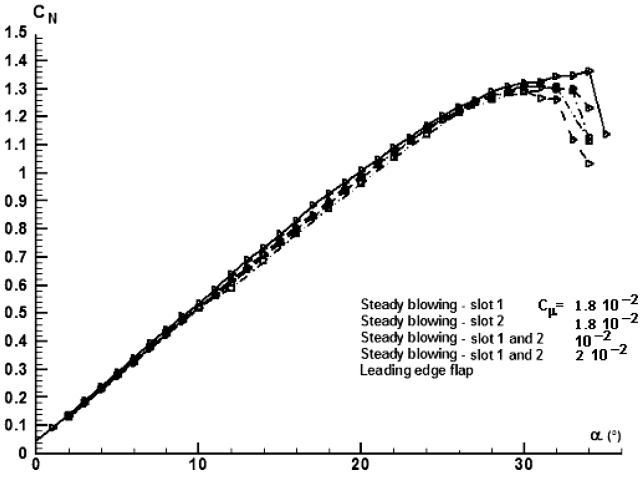

Fig. 19 Effect of leading-edge mircoflap on normal force coefficient; comparison with results obtained for full length flap, $Re_c = 1.6 \times 10^6$.

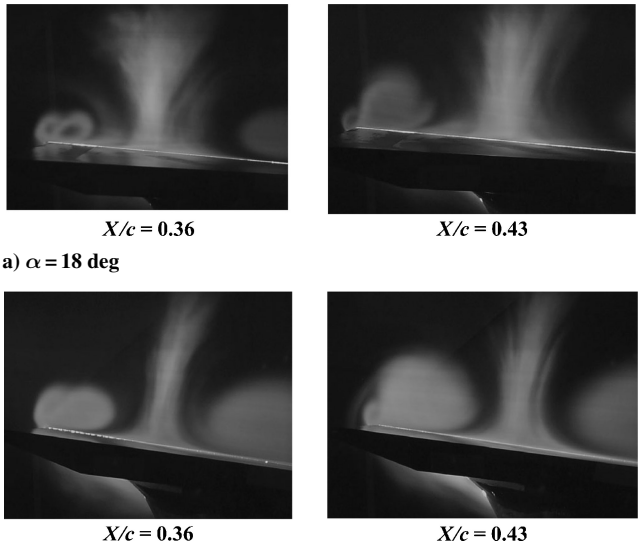

Fig. 20 Laser sheet visualizations for normal steady blowing through slots 1 and 2 and for two different incidence angles, $Re_c = 2.3 \times 10^6$ and $C_\mu = 10^{-2}$.

No significant changes are observable compared to the nominal configuration except for a blowing through slot 2 ($C_\mu = 10^{-2}$), which exhibits a small increase of C_N in the range $12 < \alpha < 21$ deg, a greater maximum value, of and a delayed stall by 1 deg in comparison with the others configurations.

Laser Sheet Visualizations

Laser sheet visualizations obtained for two angles of attack $\alpha = 18$ and 25 deg and for the same freestream Reynolds number $Re_c = 2.3 \times 10^6$ are shown in Fig. 20 for a steady normal blowing through slots 1 and 2 ($C_\mu = 5 \times 10^{-3}$). Visualizations are performed in two transverse planes: plane $X/c = 0.36$ located between both slots and plane $X/c = 0.43$ located downstream of slot 2. In each plane, a second vortex develops near the leading edge with a size comparable to that of the primary vortex. In the downstream plane, $X/c = 0.43$, another structure develops to a lesser extent. The application of control induces an earlier breakdown because for $\alpha = 18$ deg the primary vortex is braker down at $X/c = 0.43$ vs $X_b/c = 0.46$ in the nominal configuration.

LDV

Figure 21 presents the contours of the nondimensional axial vorticity component in the transverse plane, $X/c = 0.36$, for a blowing through slots 1 and 2 and for the same freestream conditions as for

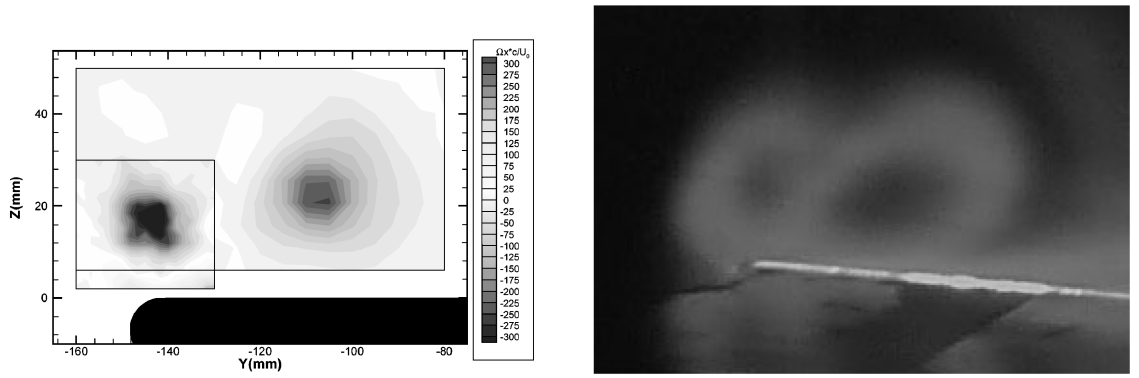

LDV **Laser sheet Visualization**

Fig. 21 Nondimensionnal axial vorticity component $\Omega_X c/U_0$ and laser sheet visualization in transverse plane $X/c = 0.36$ of normal steady blowing through slots 1 and 2, $Re_c = 2.3 \times 10^6$, $\alpha = 18$ deg, and $C_\mu = 10^{-2}$.

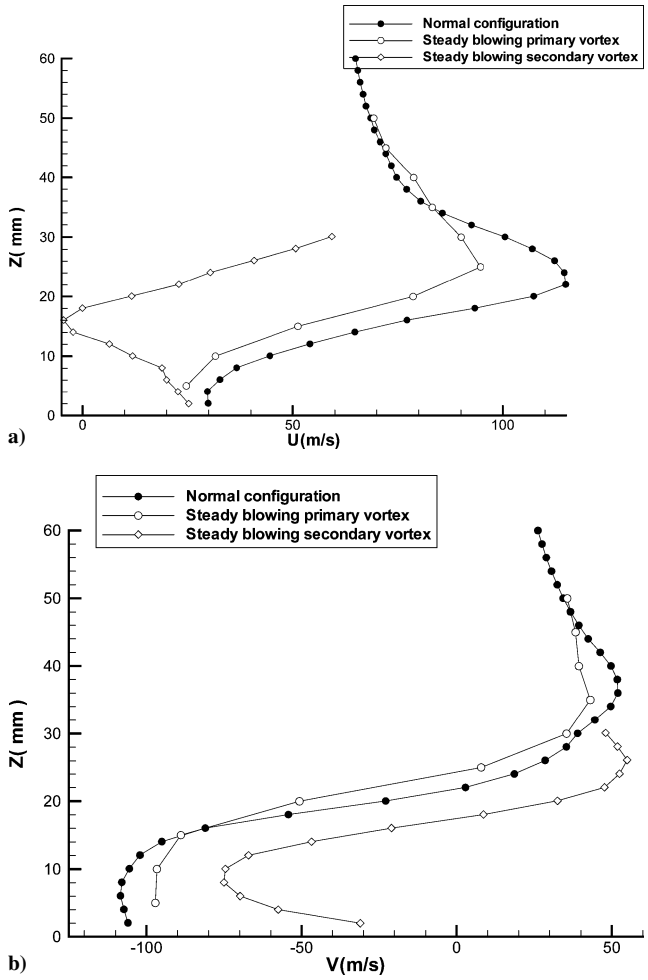

Fig. 22 Velocity profiles for normal steady blowing through slots 1 and 2 ($C_\mu = 10^{-2}$), plane at $X/C = 0.36$, $Re_c = 2.3 \times 10^6$, and $\alpha = 18$ deg: a) streamwise and b) spanwise.

the nominal configuration: $\alpha = 18$ deg and $Re_c = 2.3 \times 10^6$. The measurement plane is located between the blowing slots. Theses results are compared to an equivalent laser sheet visualization. The measurements confirm the formation of a steady vortex near the leading edge corotating with the primary vortex. The application of steady blowing does not change either the transverse position or the structure of the primary vortex, but it replaces the separated shear layer emanating from the separation line.

Figure 22 present the axial U and tangential V velocity components extracted from LDV data along a vertical plane passing through the centers of the primary vortex and of the vortex formed at the leading edge. Results are compared to the nominal primary vortex distributions. The velocity profiles are significantly modified by the control application. The acceleration of the axial velocity in the primary vortex core is reduced by the control with values reaching $U/U_0 = 1.9$ compared to $U/U_0 = 2.3$ in the nominal flow. The secondary vortex has a wake-type profile with a recirculation region in its core. Also, the spanwise velocity amplitude and an estimation of the rotation rate of the vortex on its axis (provided by the value of $\partial V/\partial Z$ in the primary vortex core) are lowered in presence of control. Note that this measure of the rotation rate is greater in the control vortex than in the primary vortex.

Conclusions

This experimental study provides a detailed characterization of the vortical flowfield over a rounded leading-edge delta wing model with a 60-deg sweep angle. It also presents steady or pulsed blowing normal to the leading edge. Surface and flowfield visualizations mean and instantaneous surface pressure, and mean velocity measurements are presented.

The nominal flow, that is, without control, is first described. The vortex breakdown phenomenon occurs earlier over the wing in comparsion with more slender delta wing models. Its progression with α toward the apex is slowed down as an effect of the rounded leading edge compared to a sharp one. Moreover, the primary separation line of the shear layer is not rectilinear along the rounded leading edge, contrary to results with a sharp leading edge. This last feature complicates the study of the flowfield and the location of the control devices. The recirculation zone downstream of the vortex breakdown location is absent, which seems to be related to the low strength of the main vortices, observed in the LDV results, with respect to more slender delta wings.

The flow control consists in a continuous or pulsed blowing normal to the leading edge with a low mean blowing coefficient $C_\mu < 2 \times 10^{-2}$. A large number of experimental configurations is analyzed. This control system does not allow a significant modification of the vortex breakdown location. However, it strongly modifies the vortical structure: A strong and steady vortex is formed in the neighborhood of the blowing slot; it is corotating with the primary vortex. The intensity and axial velocity excess in the core of the primary vortex are reduced by the control.

Neither the maximum normal force nor the stall incidence is strongly affected by the different control configurations. However, dissymmetric blowing could generate a significant rolling moment. As an example, blowing through slot 2 with a mean blowing coefficient of $C_\mu = 10^{-2}$ induces a variation of the rolling moment coefficient $\Delta C_l = 7.6 \times 10^{-3}$ at $\alpha = 17$ deg and $\Delta C_l = 1.2 \times 10^{-2}$ at $\alpha = 34$ deg. These values are greater than those obtained with a full length flap set along the leading edge and perpendicular to its surface. This change in rolling moment is a complicated function of the control parameters, but it increases with the blowing coefficient value.

Acknowledgments

The authors thank Délégation Générale pour l'Armement/ Service des Programmes Aéronautiques for their financial support. The authors express their sincerest thanks to the members of the F2 wind-tunnel team for their help in accomplishing these tests. Teams of ONERA who designed and manufactured the delta wing model and the pulsating mechanism are also acknowledged.

References

[1]Mitchell, A. M., "Caractérisation et Contrôle de l'Éclatement Tourbillonnaire sur une Aile Delta aux Hautes Incidences," Ph.D. Dissertation, Dept. de Mécanique, Univ. of Paris 6, Paris, July 2000.

[2]Mitchell, A. M., Barberis, D., Molton, P., and Gobert, J.-L., "Control of Vortex Breakdown by Along-the-Core Blowing," AIAA Paper 2000-2608, June 2000.

[3]Mitchell, A. M., Barberis, D., Molton, P., and Délery, J., "Control of Vortex Breakdown Location by Symmetric and Asymmetric Blowing," AIAA Paper 99-3652, June–July 1999.

[4]Mitchell, A. M., Barberis, D., Molton, P., and Délery, J., "Oscillation of Vortex Breakdown Location and Control of the Time-Averaged Location by Blowing," *AIAA Journal*, Vol. 38, No. 5, 2000, pp. 793–803.

[5]Barberis, D., and Molton, P., "Experimental Study of Three-Dimensional Separation on a Large Scale Model," *AIAA Journal*, Vol. 33, No. 11, 1995, pp. 2107–2113.

[6]Woods, N. J., and Roberts, L., "Control of Vortical Lift on Delta Wings by Tangential Leading-Edge Blowing," *Journal of Aircraft*, Vol. 25, No. 3, 1988, pp. 236–243.

[7]Gu, W., Robinson, O., and Rockwell, D., "Control of Vortices on a Delta Wing by Leading-Edge Injection," *AIAA Journal*, Vol. 31, No. 7, 1993, pp. 1177–1186.

[8]Barberis, D., Quélin, C., and Petit, S., "Contrôle de l'Éclatement Tourbillonnaire sur l'Aile AFV-D60° au Tunnel Hydrodynamique TH2," ONERA, Rept. 236/03582 DAFE, March 2001.

[9]Matsuno, T., Yokouchi, S., Kaiden, T., and Nakamura, Y., "Flow Control on a 45-Degree Delta Wing Using a Small Flap," AIAA Paper 2002-0124, Jan. 2002.

[10]Folk, C., and Ho, C. M., "Micro-Actuators for Control of Delta Wing with Sharp Leading-Edge," AIAA Paper 2001-0121, Jan. 2001.

[11]Ho, C. M., Huang, P. H., Yang, J. M., Lee, G. B., and Tai, Y. C., "Active Flow Control by Microsystems," Flowcon, International Union of Theoretical and Applied Mechanics Symposium on Mechanics of Passive and Active Flow Control, Sept. 1998.

[12]Jiang, F., Lee, G. B., Tai, Y. C., and Ho, C. M., "A Flexible Micromachine-Based Shear-Stress Sensor Array and Its Application to Separation-Point Detection," *Sensors and Actuators A*, Vol. 79, No. 3, 2000, pp. 194–203.

[13]Huang, A., Folk, C., Silva, C., Christensen, Y., Chen, Y., Ho, C. M., Jiang, F., Grosjean, C., Tai, Y. C., Lee, G. B., Chen, M., and Newbern, S., "Application of MEMS Devices to Delta Wing Aircraft: From Concept Development to Transonic Flight Test," AIAA Paper 2001-0124, Jan. 2001.

[14]Luckring, J. M., "Reynolds Number and Leading-Edge Bluntness Effects on a 65° Delta Wing," AIAA Paper 2002-0419, Jan. 2002.

[15]Afchain, D., Broussaud, P., Frugier, M., and Rancarani, G., "La Soufflerie F2 du Centre du Fauga-Mauzac," ONERA, TP 1983-139, No. 193880, Châtillon, France, Nov. 1983.

[16]Masure, B., Solignac, J. L., and Laval, P., "Mass Flow Rate Measurements by Means of a Sonic Throat," ONERA, TP 956, Châtillon, France, May 1971.

[17]Le Sant, Y., Deléglise, B., and Mébarki, Y., "An Automatic Image Alignment Method Applied to Pressure Sensitive Paint Measurements," ONERA, TP 1997-162, Châtillon, France, Sept.–Oct. 1997.

[18]Chanetz, B., "Contribution à l'Étude Expérimentale et Théorique de l'Éclatement Tourbillonnaire en Air Incompressible," Ph.D. Dissertation, Univ. of Lyon, Lyon, France, Sept. 1986.

[19]Obara, C. J., "Sublimating Chemical Technique for Boundary-Layer Flow Visualization in Flight Testing," *Journal of Aircraft*, Vol. 25, No. 6, 1988, pp. 493–498.

[20]Barberis, D., "D2-1 Test Case, Delta-Wing Model, A Section of Test Cases for the Validation of CFD Codes," AGARD AD Rept. 303, Aug. 1994.

[21]Wentz, W. H., and Kohlman, D. L., "Vortex Breakdown on Slender Sharp-Edged Wings," *Journal of Aircraft*, Vol. 8, No. 3, 1971, pp. 156–161.

[22]Hall, M. G., "A Theory for the Core of a Leading-Edge Vortex," *Journal of Fluid Mechanics*, Vol. 11, No. 2, 1961, pp. 209–228.

[23]Lambourne, N. C., and Bryer, D. W., "The Bursting of Leading-Edge Vortices—Some Observations and Discussion of the Phenomenon," Aeronautical Research Council, ARC R&M 3282, London, April 1961.

[24]Escudier, M. P., Bornstein, J., and Zehnder, N., "Observations and LDA Measurements of Confined Turbulent Vortex Flow," *Journal of Fluid Mechanics*, Vol. 98, No. 1, 1980, pp. 49–63.

[25]Leibovitch, S., "The Structure of Vortex Breakdown," *Annual Review of Fluid Mechanics*, Vol. 10, 1978, pp. 221–246.

[26]Mitchell, A. M., and Molton, P., "Vortical Substructures in the Shear Layers Forming Leading-Edge Vortices," *AIAA Journal*, Vol. 40, No. 8, 2002, pp. 1689–1692.

[27]Reynolds, G., and Abtahi, A., "Three Dimensional Vortex Development, Breakdown and Control," AIAA Paper 89-0998, March 1989.

[28]Payne, F. M., Ng, T. T., Nelson, R. C., and Schiff, L. B., "Visualization and Wake Surveys of Vortical Flow over a Delta Wing," *AIAA Journal*, Vol. 26, No. 2, 1988, pp. 137–143.

[29]Coton, F. N., Jupp, M. L., and Green, R. B., "Analysis of Unsteady Pressure Signals on a Pitching Delta Wing," *AIAA Journal*, Vol. 39, No. 9, 2001, pp. 1750–1757.

[30]Gursul, I., "Unsteady Flow Phenomena over Delta Wings at High Angle of Attack," *AIAA Journal*, Vol. 32, No. 2, 1994, pp. 225–231.

[31]Garg, A. K., and Leibovitch, S., "Spectral Characteristics of Vortex Breakdown Flowfields," *Physics of Fluids*, Vol. 22, No. 11, 1979, pp. 2053–2064.

[32]Leibovich, S., and Stewartson, K., "A Sufficient Condition for Instability of Columnar Vortices," *Journal of Fluid Mechanics*, Vol. 126, 1983, pp. 335–356.

[33]Renac, F., "Contrôle expérimental de l'écoulement tourbillonnaire sur une aile delta," Ph.D. Dissertation, Dept. de Mécanique, Univ. of Paris VI, Paris, April 2004.

[34]Hong, J. S., Celik, Z. Z., and Roberts, L., "Effects of Leading-Edge Lateral Blowing on Delta Wing Aerodynamics," *AIAA Journal*, Vol. 34, No. 12, 1996, pp. 2471–2478.

K. Fujii
Associate Editor